

## Tuning thermal conductivity of nanoporous crystalline silicon by surface passivation: A molecular dynamics study

Jin Fang and Laurent Pilon

Citation: *Appl. Phys. Lett.* **101**, 011909 (2012); doi: 10.1063/1.4733352

View online: <http://dx.doi.org/10.1063/1.4733352>

View Table of Contents: <http://apl.aip.org/resource/1/APPLAB/v101/i1>

Published by the [American Institute of Physics](#).

---

### Related Articles

On calculation of thermal conductivity from Einstein relation in equilibrium molecular dynamics

*J. Chem. Phys.* **137**, 014106 (2012)

Electron-dependent thermoelectric properties in Si/Si<sub>1-x</sub>Gex heterostructures and Si<sub>1-x</sub>Gex alloys from first-principles

*Appl. Phys. Lett.* **100**, 253901 (2012)

Finite element calculations of the time dependent thermal fluxes in the laser-heated diamond anvil cell

*J. Appl. Phys.* **111**, 112617 (2012)

Analysis of thermal conductance of ballistic point contacts

*Appl. Phys. Lett.* **100**, 233109 (2012)

Phononic and structural response to strain in wurtzite-gallium nitride nanowires

*J. Appl. Phys.* **111**, 103506 (2012)

---

### Additional information on *Appl. Phys. Lett.*

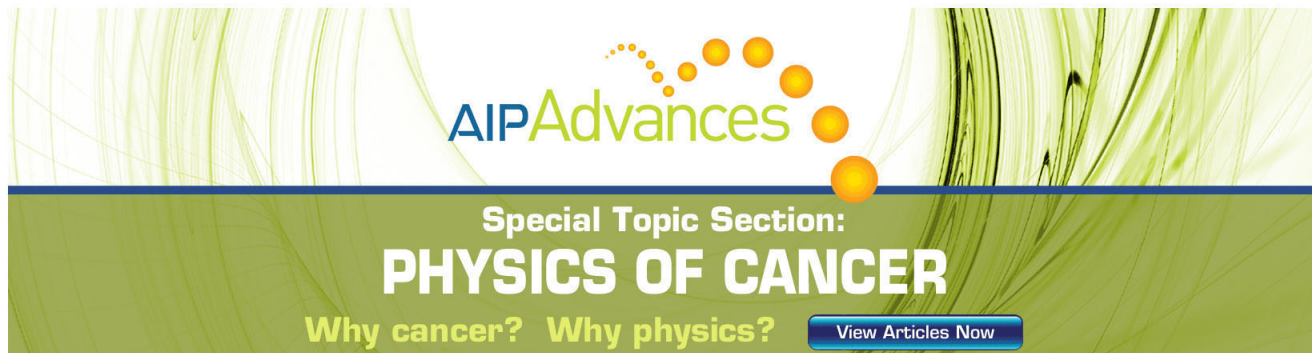
Journal Homepage: <http://apl.aip.org/>

Journal Information: [http://apl.aip.org/about/about\\_the\\_journal](http://apl.aip.org/about/about_the_journal)

Top downloads: [http://apl.aip.org/features/most\\_downloaded](http://apl.aip.org/features/most_downloaded)

Information for Authors: <http://apl.aip.org/authors>

## ADVERTISEMENT

The advertisement features a green and white background with abstract, flowing lines. At the top, the 'AIP Advances' logo is displayed, with 'AIP' in blue and 'Advances' in green, accompanied by a series of orange circles of varying sizes. Below the logo, the text 'Special Topic Section: PHYSICS OF CANCER' is written in white, with 'PHYSICS OF CANCER' in a larger, bold font. At the bottom, the phrase 'Why cancer? Why physics?' is written in green, and a blue button with the text 'View Articles Now' is positioned on the right side.

AIP Advances

Special Topic Section:  
**PHYSICS OF CANCER**

Why cancer? Why physics? [View Articles Now](#)

## Tuning thermal conductivity of nanoporous crystalline silicon by surface passivation: A molecular dynamics study

Jin Fang and Laurent Pilon<sup>a)</sup>

Mechanical and Aerospace Engineering Department, Henry Samueli School of Engineering and Applied Science, University of California-Los Angeles, 420 Westwood Plaza, Los Angeles, California 90095, USA

(Received 20 January 2012; accepted 18 June 2012; published online 5 July 2012)

Surface passivation of nanoporous crystalline silicon can reduce its thermal conductivity. This was established using equilibrium molecular dynamics simulations. The porosity varied from 8% to 38% while the pore diameter ranged from 1.74 to 2.93 nm. Hydrogen and oxygen passivation reduced thermal conductivity by 11% to 17% and 37% to 51% depending on porosity at 500 K, respectively. The hydrogen passivation effect decreased with increasing temperature. Vibrational spectra of oxygen overlapped with those of silicon at low frequencies. Therefore, oxygen passivation enhanced phonon scattering at solid matrix boundaries, resulting in stronger thermal conductivity reduction than that caused by hydrogen passivation. © 2012 American Institute of Physics. [<http://dx.doi.org/10.1063/1.4733352>]

Porous silicon is an important semiconductor material with a wide range of applications. For example, it has been used in optoelectronics for its photoluminescence properties.<sup>1</sup> It also served as thermal insulators and sensors in micro-electro-mechanical systems (MEMS) due to its low thermal conductivity and rigid solid structure.<sup>2,3</sup> In addition, nanoporous silicon was found promising in highly energetic MEMS devices such as microthrusters and microinitiators using its strong oxidation reaction.<sup>4,5</sup> More recently, nanoporous silicon was identified as a high temperature thermoelectric material for energy harvesting purposes.<sup>6,7</sup> Its low thermal conductivity  $k$ , high electrical conductivity  $\sigma$ , and high Seebeck coefficient  $S$  contribute to a high thermoelectric figure of merit  $ZT$  defined as  $ZT = \sigma S^2 T / k$  at temperature  $T$ . In all these applications, tuning the thermal conductivity of porous silicon is essential to the material design and performance.

Recently, we reported a scaling law for thermal conductivity of nanoporous crystalline silicon with unpassivated pores by combining kinetic theory and non-equilibrium molecular dynamics (NEMD) simulations.<sup>8</sup> The thermal conductivity  $k_0$  was found to be linearly proportional to  $\Psi(f_v)/(A_i/4)$ , where  $f_v$  is the porosity,  $\Psi(f_v) = 1 - 1.5f_v$  corresponds to the coherent potential effective medium approximation,<sup>9</sup> and  $A_i = 6f_v/d_p$  is the interfacial area concentration for a simple cubic pore arrangement. The pore diameter  $d_p$  ranged from 1.74 to 5.86 nm while the porosity  $f_v$  varied from 8% to 38%, corresponding to an interfacial area concentration  $A_i$  between  $0.16 \times 10^9$  and  $0.78 \times 10^9$  m<sup>2</sup>/m<sup>3</sup>.

In practice, Si atoms located at the pore surface are chemically passivated. For example, surfaces of porous silicon prepared using electrochemical etching are usually passivated with hydrogen atoms.<sup>10</sup> The hydrogen passivated surfaces, however, are easily oxidized when exposed to atmosphere or moisture, resulting in oxygen passivation. In general, surface passivation in nanostructured materials was

found to affect their chemical reactivity,<sup>11,12</sup> electrical and optical properties,<sup>13,14</sup> as well as their thermal conductivity.<sup>15–17</sup> For example, recent molecular dynamics study showed that hydrogen passivation on the edges of graphene nanoribbons reduced their thermal conductivity by about 40%–60% between 100 and 300 K.<sup>15,16</sup> This was attributed to phonon scattering by the hydrogen passivated edges.<sup>15,16</sup> In addition, Lee *et al.*<sup>6</sup> reported the room temperature thermal conductivity of hydrogen passivated nanoporous silicon with cylindrical pores using equilibrium molecular dynamics (EMD). The porosity and pore diameter varied from 7% to 38% and from 0.63 to 2.26 nm, respectively. However, the effects of the chemical nature of the passivation was not explicitly investigated. Considering the large interfacial area concentration present in nanoporous silicon, the effect of surface passivation may become significant and therefore add another parameter in the quest to tune their thermal conductivity for various applications.

In the present study, the thermal conductivity of both hydrogen and oxygen passivated nanoporous silicon was simulated using EMD.<sup>18</sup> Unlike NEMD simulations performed previously,<sup>8</sup> EMD simulations can be used to predict the bulk thermal conductivity directly with a relatively small number of atoms.<sup>18</sup> In addition, dynamic properties such as the phonon density of state can be conveniently calculated.<sup>19</sup> The Tersoff-type potential reported by de Brito Mota *et al.*<sup>20</sup> was used to simulate Si-H and H-H interatomic interactions while another Tersoff-type potential parameterized by Munetoh *et al.*<sup>21</sup> was used for Si-O and O-O interactions. The parameters for Si-Si interactions reported by Tersoff<sup>22</sup> were used for both types of passivated silicon.

Figures 1(a) and 1(b) show the surface bonding structures of hydrogen and oxygen passivation investigated in the present study, respectively. For hydrogen passivation, Si-H bonds were used to terminate the dangling bonds of the Si atoms at the pore surface. For oxygen passivation, Si-O-Si bridge bonds were applied to passivate neighboring surface Si atoms. This passivation method was also used by Lin *et al.*<sup>23</sup> recently to study the band gap of oxygen passivated

<sup>a)</sup> Author to whom correspondence should be addressed. Electronic mail: [pilon@seas.ucla.edu](mailto:pilon@seas.ucla.edu).

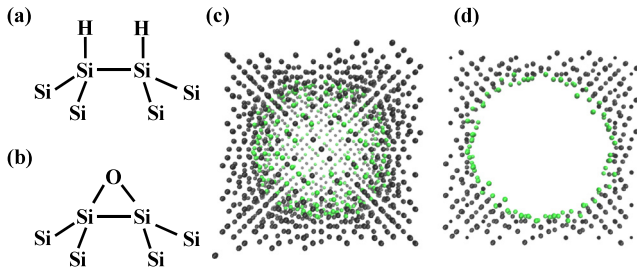


FIG. 1. Surface bonding structure for (a) hydrogen passivated and (b) oxygen passivated nanoporous crystalline silicon, along with (c) atomic structure of hydrogen passivated nanoporous silicon with 38% porosity. The green and white spheres correspond to silicon and hydrogen atoms, respectively.

Si nanonets. As an example, Figure 1(c) shows the 3D atomic structure of the simulation domain with 38% porosity. It contained  $6 \times 6 \times 6$  unit cells for a total side length  $L = 3.258$  nm. A spherical pore with diameter  $d_p$  was created by removing Si atoms within selected region of the simulation domain. Figure 1(d) shows a front view of a thin slice cut through the pore's equator and clearly illustrates surface passivation by hydrogen atoms. Periodic boundary conditions were used in all three directions corresponding to a simple cubic pore arrangement. According to Schelling *et al.*<sup>18</sup> and Lee *et al.*,<sup>6</sup> the effect of the simulation domain size was negligible for the systems investigated in the present study. This was also verified by the fact that the simulated thermal conductivity of nanoporous silicon systems at 500 K with one and two pores were identical within the simulation uncertainties. Table I summarizes the range of porosity  $f_v$ , spherical pore diameter  $d_p$ , and interfacial area concentration  $A_i$  of the different systems investigated.

To account for the surface passivation, hydrogen and oxygen atoms were placed in the vicinity of surface Si atoms at a distance of 1.50 Å and 1.60 Å corresponding to the Si-H and Si-O bond length, respectively.<sup>20,21</sup> Note that the number of the oxygen atoms was half of that of the hydrogen atoms due to the fact that one oxygen atom was connected to two silicon atoms as shown in Figure 1(b). After passivating the pore surface, an energy minimization step was performed to relax the entire structure. Simulations were performed with a time step of 0.05 fs. Initially, the system was set to equilibrium at a desired temperature by imposing constant number of atoms, volume, and temperature conditions (NVT ensemble) for 1 million time steps. Then, the system was relaxed under constant number of atoms, volume, and energy conditions (NVE ensemble) for another 1 million time steps. Finally, the thermal conductivity was estimated based on the Green-Kubo relation expressed as,<sup>18</sup>

$$k = \frac{1}{3Vk_B T} \int_0^{\tau_M} \langle J(0)J(t) \rangle dt, \quad (1)$$

where  $V$  is the volume of the system,  $k_B = 1.38 \times 10^{-23}$  J/K is the Boltzmann constant,  $T$  is the temperature in K,  $\langle J(0)J(t) \rangle$  is the time-averaged heat current autocorrelation function (HCACF), and  $\tau_M$  is the maximum length of correlation time window. The details of the Green-Kubo methodology can be found in Ref. 18.

In the present study, the HCACF decayed with time and oscillated around zero when  $t > 30$  ps for nanoporous crystalline silicon. Therefore, the integral in Eq. (1) converged for  $\tau_M > 30$  ps. The integral was averaged over numerous time windows with  $\tau_M$  ranging between 30 ps and 80 ps. Then, it was used to determine the thermal conductivity from Eq. (1). In addition, the total simulation time should be considerably larger than  $\tau_M$  in order to achieve good statistical averaging of the HCACF and accurate thermal conductivity predictions.<sup>18</sup> We found that the thermal conductivity reached a plateau when the total simulation time was 2 ns or larger. Therefore, a total simulation time of 2 ns, corresponding to 40 million time steps, was adopted for all simulations. Finally, for each system and temperature, the average thermal conductivity and the associated uncertainty corresponding to 95% confidence intervals were estimated from 12 independent simulations.

For validation purposes, the thermal conductivity of dense (nonporous) crystalline silicon denoted by  $k_b$  was simulated and found to be  $120 \pm 13$ ,  $79 \pm 9$ , and  $57 \pm 6$  W/m·K at 500, 750, and 1000 K, respectively. These values were in good agreement with NEMD results recently reported by Abs da Cruz *et al.*<sup>24</sup> Note that, according to Volz and Chen,<sup>25</sup> quantum corrections are negligible for crystalline silicon systems beyond 500 K.

Figures 2(a) and 2(b) show the thermal conductivity of hydrogen and oxygen passivated nanoporous crystalline silicon, denoted as  $k_{HP}(T)$  and  $k_{OP}(T)$ , as a function of temperature from 500 to 1000 K, respectively. The thermal conductivity of unpassivated nanoporous silicon  $k_0(T)$  was also plotted for comparison purposes. It is evident that thermal conductivity of all nanoporous silicon systems decreased with increasing porosity. For example, thermal conductivity of unpassivated nanoporous silicon at 500 K decreased from  $9.09 \pm 0.92$  to  $1.47 \pm 0.17$  W/m·K when porosity increased from 8% to 38% at 500 K. Overall, the presence of nanopores reduced thermal conductivity of dense crystalline silicon by about one order of magnitude at all temperatures. The thermal conductivity of nanoporous crystalline silicon has been shown to decrease not only due to the loss of material, taken into account by effective medium approximation, but also by strong phonon scattering at pore surface.<sup>6,8,26</sup> In fact, we verified that the scaling law  $k \propto (1 - 1.5f_v)/(A_i/4)$  previously reported<sup>8</sup> was also applicable to the passivated nanoporous crystalline silicon.

In addition, Figures 2(a) and 2(b) show that the simulated thermal conductivity for passivated and unpassivated systems decreased monotonically with increasing temperature from 500 to 1000 K for porosity less than 27%. This can be attributed to the fact that phonon Umklapp scattering, caused by anharmonic interactions, increased with increasing

TABLE I. Summary of nanoporous crystalline silicon systems with spherical pores in simple cubic arrangement for various porosity  $f_v$ , pore diameter  $d_p$ , and interfacial area concentration  $A_i$ .

Sample No.	Porosity $f_v$ (%)	Pore diameter $d_p \times 10^{-9}$ (m)	Interfacial area concentration $A_i \times 10^9$ (m <sup>2</sup> /m <sup>3</sup> )
1	8	1.74	0.28
2	15	2.17	0.42
3	27	2.61	0.62
4	38	2.93	0.78

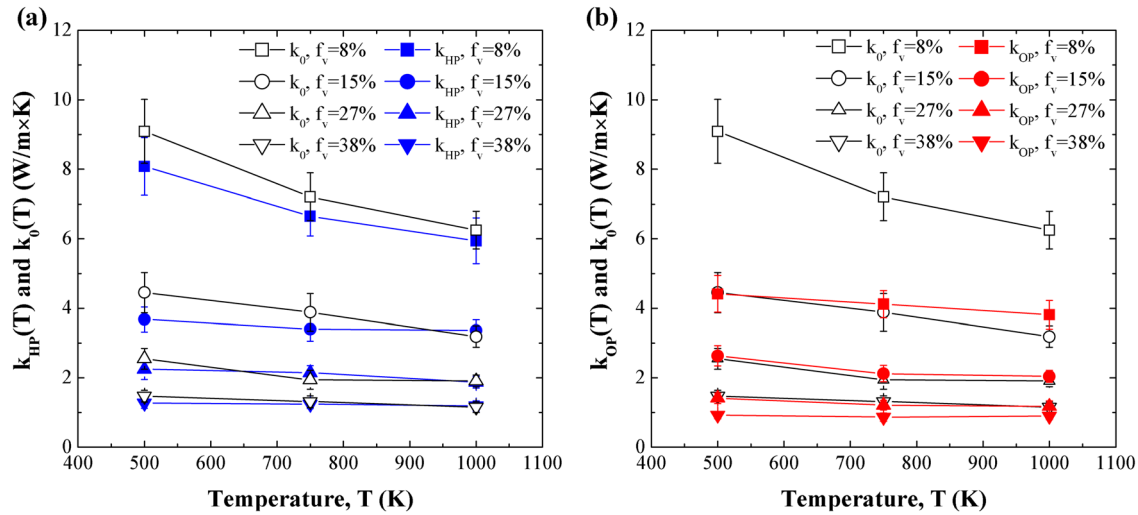


FIG. 2. Thermal conductivity of (a) hydrogen passivated nanoporous crystalline silicon denoted by  $k_{HP}(T)$  and (b) oxygen passivated nanoporous crystalline silicon denoted by  $k_{OP}(T)$ , as a function of temperature from 500 to 1000 K, respectively. Thermal conductivity of unpassivated nanoporous silicon  $k_0(T)$  was also shown for comparison.

temperature. However, the thermal conductivity of systems with porosity of 27% and 38% did not clearly exhibit such temperature dependency. This can be attributed to the fact that strong phonon scattering by pores boundaries and passivation layers dominated over Umklapp scattering. Finally, it is evident that oxygen passivation reduced thermal conductivity of nanoporous crystalline silicon while hydrogen passivation had a lesser effect.

Figures 3(a) and 3(b) plot the ratios  $k_{HP}(T)/k_0(T)$  and  $k_{OP}(T)/k_0(T)$  as a function of porosity at 500, 750, and 1000 K, respectively. Note that the increasing error bars with porosity was caused by the small value of  $k_0(T)$  for systems with large porosity, according to standard error propagation analysis. It is evident that the presence of hydrogen passivation reduced the thermal conductivity at 500 K by 11% to 17% depending on the porosity. On the other hand, oxygen passivation reduced the thermal conductivity at 500 K by 37% to 51%. The reduction was attributed to phonon scattering by the passivated surfaces, including the Si atoms at the pore surface and passivation atoms. In addition, hydrogen

passivation did not have a statistically significant effect on the thermal conductivity at 750 K and 1000 K for all porosities as shown in Figure 3(a). In fact, hydrogen passivation effect was masked by strong phonon Umklapp scattering at high temperatures. However, statistically significant reduction in thermal conductivity was observed for oxygen passivated nanoporous silicon for all porosities and temperatures investigated. Finally, note that phonon leakage, such as that observed in Si supported graphene sheets and resulting in low thermal conductivity,<sup>27–29</sup> was not expected in the present nanoporous crystalline silicon since the pores were empty.

To further understand the origin of thermal conductivity reduction in passivated nanoporous silicon, we considered the vibrational spectra obtained by Fourier transform of the velocity autocorrelation function.<sup>19</sup> Figure 4(a) shows the vibrational spectra of the hydrogen passivated, oxygen passivated, and unpassivated Si atoms located at the pore surface in the nanoporous system with 8% porosity at 500 K. The vibrational spectrum or the phonon density of states of bulk

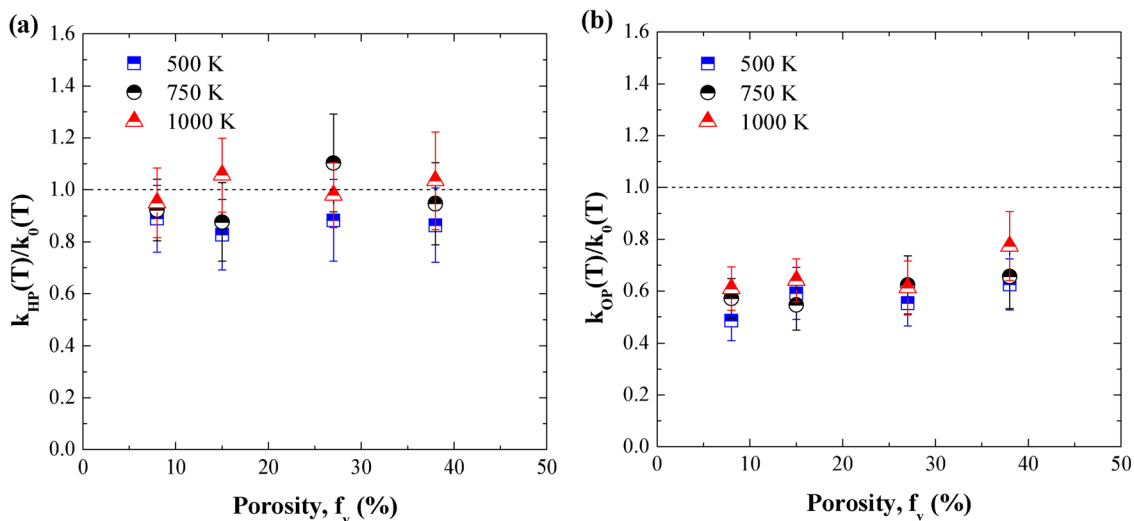


FIG. 3. Ratios  $k_{HP}(T)/k_0(T)$  and  $k_{OP}(T)/k_0(T)$  as a function of porosity at 500, 750, and 1000 K, respectively. Here,  $k_{HP}(T)$ ,  $k_{OP}(T)$ , and  $k_0(T)$  denote the thermal conductivity of hydrogen passivated, oxygen passivated, and unpassivated nanoporous silicon, respectively.

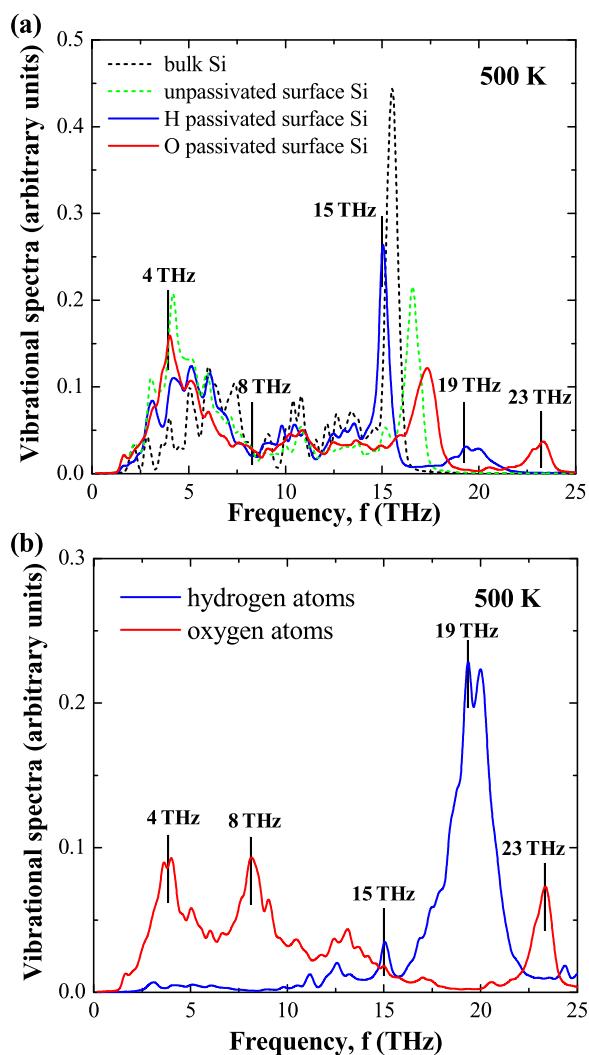


FIG. 4. (a) Vibrational spectra of hydrogen passivated, oxygen passivated, and unpassivated surface Si atoms in nanoporous silicon at 500 K with 8% porosity. The phonon density of states of bulk crystalline silicon is also shown as a reference. (b) Vibrational spectra of surface hydrogen and oxygen atoms in nanoporous silicon at 500 K with 8% porosity.

silicon is also shown as a reference. The peaks present at frequencies less than 12 THz and around 13–18 THz for all spectra correspond to acoustic and optical modes, respectively.<sup>30,31</sup> Note that acoustic phonons contribute to heat transport unlike optical phonons which mainly affect optical properties.<sup>32</sup> It is evident that the acoustic modes of both passivated and unpassivated surface Si atoms shifted to lower frequency compared with that of the bulk Si atoms. This can be attributed to the fact that the surface Si atoms have fewer Si-Si bonds than the bulk Si atoms and therefore have less stiff bonds, resulting in the softening of the phonon frequency.<sup>30,31</sup> In addition, the amplitude of the vibrational spectra in the acoustic branch of the hydrogen and oxygen passivated Si atoms were smaller than those of the unpassivated Si atoms but still larger than those of the bulk Si atoms. This can be attributed to the fact that (1) the surface passivation reduced the system's total energy by removing free bonds at the pore surfaces<sup>30,33</sup> and (2) the surface Si-O and Si-H bonds were different from the Si-Si bonds in bulk crystalline matrix. For example, the average lengths of Si-O

and Si-H bonds at the pore surface were 1.6 Å and 1.4 Å while it was 2.3 Å for Si-Si bonds in the matrix. Finally, the difference in vibrational spectra between bulk and passivated surface Si atoms also suggested that they had different lattice structures and therefore a lattice mismatch near the pore surface, resulting in additional phonon scattering.

Moreover, Figure 4(b) shows the vibrational spectra of hydrogen and oxygen atoms in the same nanoporous system with 8% porosity at 500 K. On the one hand, the oxygen atoms vibrated primarily at frequencies less than 15 THz and the amplitudes peaked around 4 and 8 THz. It is evident that the vibrational spectrum of the oxygen atoms overlapped with those of the Si atoms at low frequencies populated by acoustic phonons. This suggested that the oxygen atoms interacted and exchanged energy primarily with silicon acoustic phonons through stretching-like vibrations of Si-O bonds.<sup>34</sup> The same mechanism was also found responsible for the thermal conductivity reduction in water-filled carbon nanotubes<sup>35,36</sup> as well as in hydrogen functionalized graphene sheets.<sup>17</sup> On the other hand, Figure 4(b) shows that the hydrogen atoms vibrated primarily at frequencies larger than 15 THz and had peak amplitudes around 20 THz. Therefore, interaction and energy transfer between silicon and hydrogen atoms were reduced compared with oxygen passivation. Thus, the thermal conductivity of nanoporous Si was less affected by hydrogen passivation. Note that these results and discussion also applied to other systems and temperatures investigated.

Moreover, the vibrations of the passivation atoms at high frequencies also affected the optical modes of surface Si atoms. For example, the peaks around 15, 19, and 23 THz in the vibrational spectra of passivated surface silicon atoms [Figure 4(a)] were caused by energy transfer of the vibrational modes of the oxygen and hydrogen passivation atoms through Si-H and Si-O bonds as observed in Figure 4(b) for the same frequencies.

To conclude, the present study shows that oxygen passivation reduced the thermal conductivity of nanoporous crystalline silicon by 37% to 51% while hydrogen passivation resulted in a 11% to 17% reduction at 500 K. The hydrogen passivation effect diminished with increasing temperature. Physical mechanism responsible for the thermal conductivity reduction was investigated using the vibrational spectra of the passivation atoms and silicon atoms. Unlike for hydrogen passivation, the vibrational spectrum of oxygen atoms overlapped with those of silicon atoms at low frequencies, indicating strong interactions and energy exchange between silicon and oxygen atoms. These results can be used in designing nanostructured silicon with desired thermal conductivity by tuning not only their morphology but also their surface passivation.

This material is based upon work supported by the National Science Foundation under Grant CTS 0449429. The simulations were implemented using the Large-scale Atomic/Molecular Massively Parallel Simulator (LAMMPS) on the Hoffman2 cluster at the University of California-Los Angeles.

<sup>1</sup>A. G. Cullis, L. T. Canham, and P. D. J. Calcott, *J. Appl. Phys.* **82**, 909 (1997).

- <sup>2</sup>P. Roussel, V. Lysenko, B. Remaki, G. Delhomme, A. Dittmar, and D. Barbier, *Sens. Actuators, A* **74**, 100 (1999).
- <sup>3</sup>N. K. Ali, M. R. Hashim, and A. A. Aziz, *Solid-State Electron.* **52**, 1071 (2008).
- <sup>4</sup>F. V. Mikulec, J. D. Kirtland, and M. J. Sailor, *Adv. Mater.* **14**, 38 (2002).
- <sup>5</sup>C. R. Becker, S. Apperson, C. J. Morris, S. Gangopadhyay, L. J. Currano, W. A. Churaman, and C. R. Stoldt, *Nano Lett.* **11**, 803 (2011).
- <sup>6</sup>J. H. Lee, J. C. Grossman, J. Reed, and G. Galli, *Appl. Phys. Lett.* **91**, 223110 (2007).
- <sup>7</sup>J. H. Lee, G. A. Galli, and J. C. Grossman, *Nano Lett.* **8**, 3750 (2008).
- <sup>8</sup>J. Fang and L. Pilon, *J. Appl. Phys.* **110**, 064305 (2011).
- <sup>9</sup>R. Landauer, *J. Appl. Phys.* **23**, 779 (1952).
- <sup>10</sup>J. H. Song and M. J. Sailor, *Comments Inorg. Chem.* **21**, 69 (1999).
- <sup>11</sup>S. Ramalingam, D. Maroudas, and E. S. Aydil, *J. Appl. Phys.* **84**, 3895 (1998).
- <sup>12</sup>T. Hawa and M. R. Zachariah, *Phys. Rev. B* **69**, 035417 (2004).
- <sup>13</sup>X. Chen, X. Pi, and D. Yang, *J. Phys. Chem. C* **114**, 8774 (2010).
- <sup>14</sup>A. Miranda, F. A. Serrano, R. Vázquez-Medina, and M. Cruz-Irisson, *Int. J. Quantum Chem.* **110**, 2448 (2010).
- <sup>15</sup>W. J. Evans, L. Hu, and P. Keblinski, *Appl. Phys. Lett.* **96**, 203112 (2010).
- <sup>16</sup>J. Hu, S. Schiffli, A. Vallabhaneni, X. Ruan, and Y. P. Chen, *Appl. Phys. Lett.* **97**, 133107 (2010).
- <sup>17</sup>S.-K. Chien, Y.-T. Yang, and C.-K. Chen, *Appl. Phys. Lett.* **98**, 033107 (2011).
- <sup>18</sup>P. K. Schelling, S. R. Phillpot, and P. Keblinski, *Phys. Rev. B* **65**, 144306 (2002).
- <sup>19</sup>J. M. Dickey and A. Paskin, *Phys. Rev.* **188**, 1407 (1969).
- <sup>20</sup>F. de Brito Mota, J. F. Justo, and A. Fazzio, *J. Appl. Phys.* **86**, 1843 (1999).
- <sup>21</sup>S. Munetoh, T. Motooka, K. Moriguchi, and A. Shintani, *Comput. Mater. Sci.* **39**, 334 (2007).
- <sup>22</sup>J. Tersoff, *Phys. Rev. B* **38**, 9902 (1988).
- <sup>23</sup>L. Lin, D. Li, and J. Feng, *Nanoscale Res. Lett.* **4**, 409 (2009).
- <sup>24</sup>C. Abs da Cruz, K. Termentzidis, P. Chantrenne, and X. Kleber, *J. Appl. Phys.* **110**, 034309 (2011).
- <sup>25</sup>S. G. Volz and G. Chen, *Phys. Rev. B* **61**, 2651 (2000).
- <sup>26</sup>F. X. Alvarez, D. Jou, and A. Sellitto, *Appl. Phys. Lett.* **97**, 033103 (2010).
- <sup>27</sup>P. G. Klemens, *Int. J. Thermophys.* **22**, 265 (2001).
- <sup>28</sup>J. H. Seol, I. Jo, A. L. Moore, L. Lindsay, Z. H. Aitken, M. T. Pettes, X. Li, Z. Yao, R. Huang, D. Broido, N. Mingo, R. S. Ruoff, and L. Shi, *Science* **328**, 213 (2010).
- <sup>29</sup>R. Prasher, *Science* **328**, 185 (2010).
- <sup>30</sup>Z. Tang and N. R. Aluru, *Phys. Rev. B* **74**, 235441 (2006).
- <sup>31</sup>T.-M. Chang, C.-C. Weng, and M.-J. Huang, *J. Electron. Mater.* **39**, 1616 (2010).
- <sup>32</sup>C. L. Tien, A. Majumdar, and F. M. Gerner, *Microscale Energy Transport* (Taylor and Francis, Washington, DC, 1998).
- <sup>33</sup>T. Hawa and M. R. Zachariah, *J. Phys. Chem. C* **112**, 14796 (2008).
- <sup>34</sup>R. Soulaïrol and F. Cleri, *Solid-State Sci.* **12**, 163 (2010).
- <sup>35</sup>C. F. Carlborg, J. Shiomi, and S. Maruyama, *Phys. Rev. B* **78**, 205406 (2008).
- <sup>36</sup>J. A. Thomas, R. M. Iutzu, and A. J. H. McGaughey, *Phys. Rev. B* **81**, 045413 (2010).